ARTICLES
PUBLISHED ONLINE: 15 AUGUST 2016 | DOI: 10.1038/NNANO.2016.138
nature nanotechnology

# Rapid water disinfection using vertically aligned $MoS_2$ nanofilms and visible light

Chong Liu[1], Desheng Kong[1], Po-Chun Hsu[1], Hongtao Yuan[1], Hyun-Wook Lee[1], Yayuan Liu[1], Haotian Wang[2], Shuang Wang[3], Kai Yan[1], Dingchang Lin[1], Peter A. Maraccini[4], Kimberly M. Parker[4], Alexandria B. Boehm[4] and Yi Cui[1,5]*

**Solar energy is readily available in most climates and can be used for water purification. However, solar disinfection of drinking water mostly relies on ultraviolet light, which represents only 4% of the total solar energy, and this leads to a slow treatment speed. Therefore, the development of new materials that can harvest visible light for water disinfection, and so speed up solar water purification, is highly desirable. Here we show that few-layered vertically aligned $MoS_2$ (FLV-$MoS_2$) films can be used to harvest the whole spectrum of visible light (~50% of solar energy) and achieve highly efficient water disinfection. The bandgap of $MoS_2$ was increased from 1.3 to 1.55 eV by decreasing the domain size, which allowed the FLV-$MoS_2$ to generate reactive oxygen species (ROS) for bacterial inactivation in the water. The FLV-$MoS_2$ showed a ~15 times better log inactivation efficiency of the indicator bacteria compared with that of bulk $MoS_2$, and a much faster inactivation of bacteria under both visible light and sunlight illumination compared with the widely used $TiO_2$. Moreover, by using a 5 nm copper film on top of the FLV-$MoS_2$ as a catalyst to facilitate electron–hole pair separation and promote the generation of ROS, the disinfection rate was increased a further sixfold. With our approach, we achieved water disinfection of >99.999% inactivation of bacteria in 20 min with a small amount of material (1.6 mg $l^{-1}$) under simulated visible light.**

Rapid and energy-efficient water disinfection methods are urgently required to address global challenges related to energy and water scarcity[1–5]. Solar energy is an attractive renewable-energy resource and can be used for water disinfection via the solar disinfection of drinking water (SODIS), an approach employed throughout the world (particularly in developing countries that lack distribution systems for potable water) to disinfect water for consumption[6]. Sunlight can inactivate microorganisms via direct or indirect mechanisms. Direct mechanisms involve photons (usually ultraviolet B (UVB) or ultraviolet A (UVA)) that interact directly with nucleic acids or other essential macromolecules to cause inactivation. Indirect mechanisms involve photons (ultraviolet or visible) that interact with chromophores either within the organism or external to the organism to create reactive oxygen species (ROS) that subsequently cause inactivation. To date, most studies suggest that disinfection by ultraviolet photons is one of the most important means of inactivating waterborne pathogens[7–9]. However, energy in UVA and UVB collectively only accounts for 4% of the energy in the solar spectrum, so SODIS is time consuming (requires 6–48 h of exposure time)[6]. It is desirable to harness more effectively the energy in photons from the visible range to speed up the photoinactivation.

One way is to use a semiconductor-based photocatalyst[10–12]. When a photocatalyst absorbs light, it generates electron–hole pairs so that electrons and holes can react with water and dissolved oxygen separately to generate ROS. ROS, such as the hydroxyl radical, singlet oxygen and superoxide, are strong oxidants and can disinfect pathogens by damaging essential macromolecules[13,14]. Technically, the potentials (versus normal hydrogen electrode) for ROS production (pH 7) at the electron side for oxygen reductions are −0.33 V ($O_2/O_2^{\bullet-}$) and 0.28 V ($O_2/H_2O_2$), and at the hole side for water oxidation are 1.1–1.9 V ($H_2O/OH^{\bullet}$) and 0.82 V ($H_2O/O_2$)[15–18] (Fig. 1a), and so it is possible for an efficient photocatalyst to use the whole visible-light range of the solar spectrum. However, the bandgaps of the most-studied metal oxide photocatalysts are typically too large for most of the visible part of the solar spectrum to be utilized. For example, $TiO_2$ has a bandgap of 3.0–3.2 eV and only harvests ultraviolet light[19]. Lowering the bandgap of $TiO_2$ and enabling its absorption of visible light usually involves complex synthesis, such as doping with nitrogen, sulfur or iron[19–24], making hybrid composites of $TiO_2$ with lower bandgap materials[25,26] and advanced structural design[27,28], which limit its practical utility for photocatalytic applications[29,30]. Besides lowering the bandgap of metal oxides, research has investigated the potential for new semiconductor materials with small bandgaps, such as $C_3N_4$ (2.7 eV, cutoff wavelength 459 nm)[31,32] and red phosphorus (1.42 eV, cutoff wavelength 873 nm)[33] as photocatalysts that utilize visible light. The disinfection efficacy, specifically the disinfection rate, of these materials is still far from practical applications[25,31,34–37]. To seek novel photocatalysts that can harvest visible light for fast water disinfection is extremely attractive.

$MoS_2$, a prototypical layered transition-metal dichalcogenide, is an emerging semiconductor material with physical and chemical properties conducive to applications in transistors and electrocatalysts for hydrogen-evolution reactions[38–42]. Single- or few-layered sheets of $MoS_2$ exhibit intriguing properties distinct from those of bulk $MoS_2$. By decreasing the thickness of $MoS_2$ to a few layers or a single layer, its bandgap changes from an indirect bandgap of 1.3 eV to a direct bandgap of 1.9 eV (ref. 43). Also, nanostructured $MoS_2$ would benefit the separation of electron–hole pairs by decreasing the distances for electrons and holes to diffuse to the

[1]Department of Materials Science and Engineering, Stanford University, Stanford, California 94305, USA. [2]Department of Applied Physics, Stanford University, Stanford, California 94305, USA. [3]Department of Electrical Engineering, Stanford University, Stanford, California 94305, USA. [4]Department of Civil and Environmental Engineering, Stanford University, Stanford, California 94305, USA. [5]Stanford Institute for Materials and Energy Sciences, SLAC National Accelerator Laboratory, 2575 Sand Hill Road, Menlo Park, California 94305, USA. *e-mail: yicui@stanford.edu

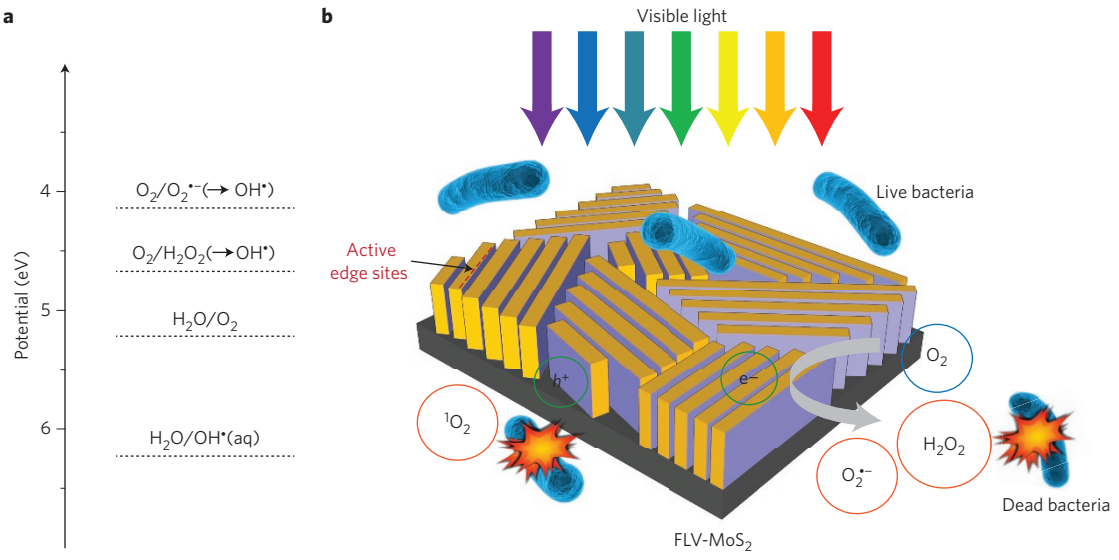


**Figure 1 | FLV-$MoS_2$ disinfection schematic. a**, The ROS-formation potentials with respect to the vacuum level. **b**, Schematic that shows the FLV-$MoS_2$ inactivating bacteria in water through visible-light photocatalytic ROS generation.

surface of the materials and also increasing the reaction sites[44]. Here we report the successful use of few-layered vertically aligned $MoS_2$ (FLV-$MoS_2$) as a photocatalyst for water disinfection under visible-light illumination (Fig. 1b). The FLV-$MoS_2$ has great potential for photocatalytic water disinfection owing to its low cost and straightforward synthesis. FLV-$MoS_2$ showed a much faster disinfection rate than $TiO_2$ under both visible-light and sunlight illumination. As semiconductor materials are nonspecific in catalysing ROS production among other competing reactions (such as hydrogen evolution, oxygen reduction and oxidation), additional catalysts (Cu or Au) were deposited onto the $MoS_2$ films to promote the production of ROS. With 5 nm of Cu or Au as both the reaction catalyst and to facilitate the separation of electron–hole pairs, FLV-$MoS_2$ achieved a rapid water disinfection with 5 log (>99.999%) inactivation of *E. coli* within 20 or 60 min, respectively, compared with that of pristine FLV-$MoS_2$ of 120 min.

## Growth and characterization of FLV-$MoS_2$

The FLV-$MoS_2$ was grown by first sputtering Mo film on a glassy carbon (GC) substrate, which was then sulfurized at 500 °C for 10 min (ref. 41). The sulfurization was conducted in a sulfur-rich environment and the $MoS_2$ film thickness was determined by the initial thickness of the Mo film sputtered. Transmission electron microscopy (TEM) images of the 40 nm $MoS_2$ film are shown in Fig. 2a. It is clear that the as-grown $MoS_2$ film is composed of vertically aligned layers of $MoS_2$ with domain sizes of around 3–10 layers, as also shown in our previous studies[41,42]. Reports have demonstrated that $MoS_2$ has a higher in-plane electrical conductivity[40,41] and also a higher catalytic activity on the edge sites, which means this vertically aligned structure can have a better electron–hole transport from $MoS_2$ to the electrolytes. For photoelectrochemical reactions, the material band structure is the key factor that directly determines the mechanism, products and efficiency. Therefore, the properties of the vertically aligned $MoS_2$ were characterized. First, the bandgap was characterized by measuring the absorption spectrum of $MoS_2$, as shown in Fig. 2b for 40 nm $MoS_2$. The bandgap value was extracted from the relation between the absorption coefficient and photon energy for the indirect bandgap semiconductor. The plot of $(\alpha h\nu)^{1/2}$ versus $h\nu$ is shown in Supplementary Fig. 1. The bandgap extraction gives 1.55 eV for 40 nm FLV-$MoS_2$. This allows FLV-$MoS_2$ to absorb light up to 800 nm wavelength and the solar spectrum utilization is also increased to ~50% in energy compared with the 4% of $TiO_2$. The Fermi level of FLV-$MoS_2$ was characterized by scanning Kelvin probe force microscopy and the results are shown in Fig. 2c–e. The Au line was patterned on the $MoS_2$ film as a reference because it has a stable work function of 5.1 eV. Figure 2d shows the line-scan data on the $MoS_2$ film that crosses the Au pattern. The Fermi level of $MoS_2$ on the line scan ranges from 5.23 to 5.26 eV with an average of 5.24 eV. The Fermi-level mapping on a $1.5 \times 12$ mm$^2$ area (Fig. 2e) shows the uniformity of the as-grown FLV-$MoS_2$ film and the averaging Fermi level across the entire area is ~5.24 eV. The valence band (VB) position of FLV-$MoS_2$ was confirmed as 5.55 eV using ultraviolet photoelectron spectroscopy and the results are shown in Supplementary Fig. 2. The band position of FLV-$MoS_2$ with respect to the ROS reaction potential and the band position of bulk $MoS_2$ are shown in Fig. 2f. The VB position for bulk $MoS_2$ is 5.54 eV (Supplementary Fig. 2). It is clear that FLV-$MoS_2$ is suitable for ROS generation for photocatalytic water disinfection.

## Photocatalytic disinfection performance of FLV-$MoS_2$

The photocatalytic disinfection performance of FLV-$MoS_2$ was then examined. First, the photocatalytic effect of FLV-$MoS_2$ was confirmed by comparing the inactivation efficiencies of bacteria with FLV-$MoS_2$ under visible light (without UVA and UVB) to those of the controls—FLV-$MoS_2$ incubated with bacteria in the dark, and visible-light illumination of the bacterial suspension without FLV-$MoS_2$. A solar simulator equipped with an ultraviolet-blocking filter was used as the light source. The Gram negative bacterium *E. coli* was used as a process indicator in all the experiments unless otherwise specified. The bacterial concentration at each time point of the experiment was normalized to the starting concentration at time 0 and the results are shown in Fig. 3a. Visible light alone or FLV-$MoS_2$ in the dark both showed <50% disinfection efficiency after 120 min, whereas FLV-$MoS_2$ under visible light showed >99.999% *E. coli* inactivation in 120 min, after which the bacteria could not be detected and no recovery was observed (Supplementary Fig. 3). The disinfection efficiency of FLV-$MoS_2$ was also compared with that of an equal mass of bulk $MoS_2$ (suspended flakes of ~2 μm) under the same experimental conditions (Fig. 3b). Bulk $MoS_2$ showed a 54% efficiency over 120 min, which is much lower than that of FLV-$MoS_2$ of >99.999%. This suggests that decreasing the size of $MoS_2$ to only a few layers

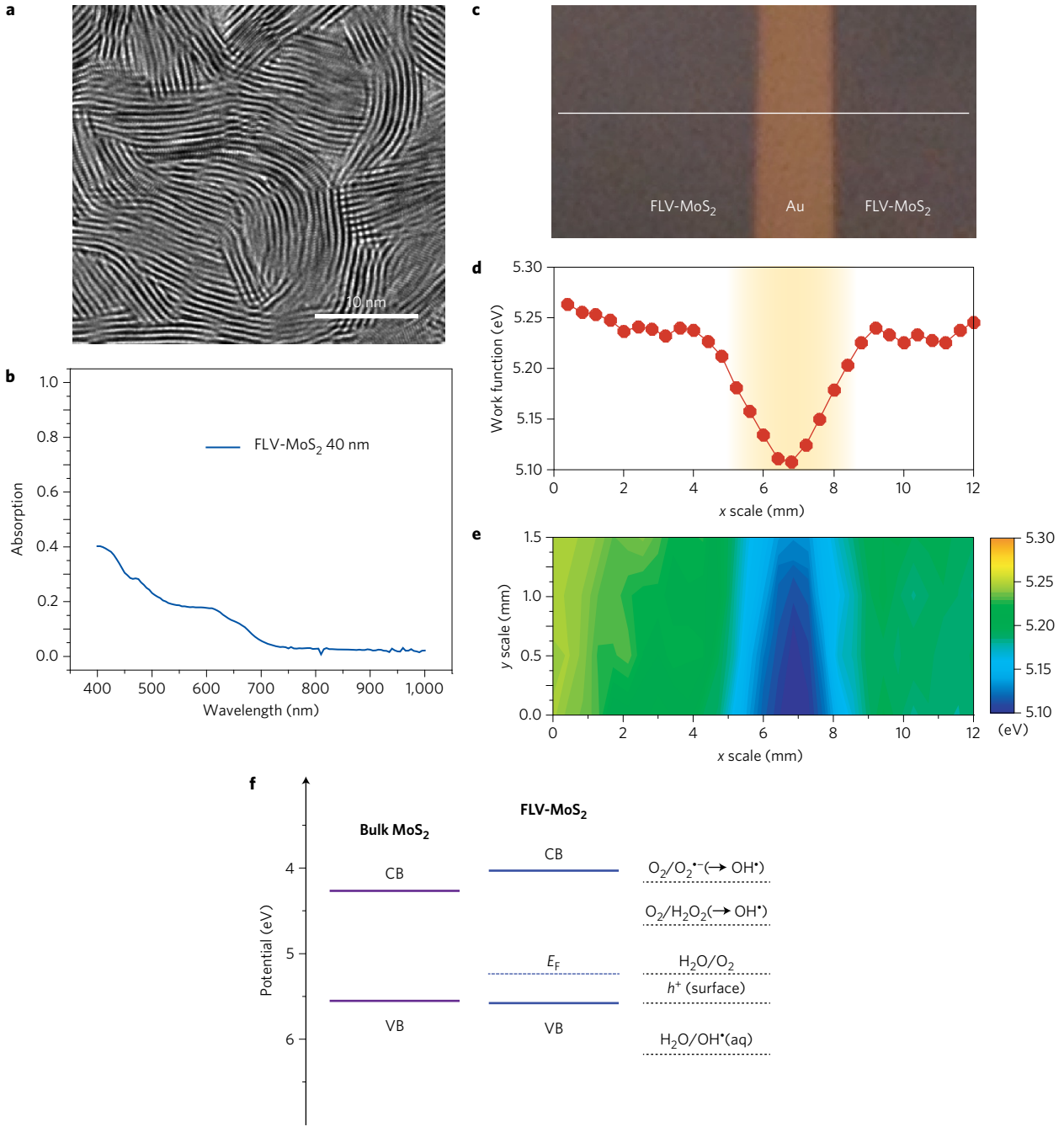


**Figure 2 | FLV-$MoS_2$ morphology and band-structure characterization. a**, TEM image (top view) of FLV-$MoS_2$ shows the as-grown vertically standing layers. **b**, Absorption spectrum of 40 nm FLV-$MoS_2$. **c**, Photograph of the FLV-$MoS_2$ film patterned with the Au line for the scanning Kelvin probe measurement. **d**, Line-scan data show the Fermi level ($E_F$) of FLV-$MoS_2$ at each position on the white line in **c**. **e**, Mapping of the FLV-$MoS_2$ film shows the Fermi level of each point on the film. **f**, The band position of FLV-$MoS_2$ with respect to the ROS formation potential and the bulk $MoS_2$ band position. CB, conduction band.

(~2–6 nm thick) can increase the photocatalyst properties of $MoS_2$. Decreasing the layer thickness of $MoS_2$ increases the ROS generation because of both the bandgap widening and the diffusion-distance shortening of the electrons and holes to the material surface. Also, the disinfection performance was compared between an equal mass of FLV-$MoS_2$ and horizontal $MoS_2$ film (Fig. 3b). The horizontal $MoS_2$ film was made of stacked $MoS_2$ nanoflakes, with each flake 1–6 nm in thickness. As both samples have larger bandgaps than that of bulk $MoS_2$, the disinfection rates were much higher. Between the FLV-$MoS_2$ and horizontal $MoS_2$, the vertical direction configuration gave a higher disinfection rate. This could be the result of a higher in-plane conductivity of the electron/hole in $MoS_2$ and also to more active edge sites exposed on the FLV-$MoS_2$ film.

To eliminate the thermal effect potentially caused by infrared light, the disinfection efficiency of *E. coli* in water with FLV-$MoS_2$ under visible light combined with infrared light and under only infrared light was compared. The light spectrum is shown in Fig. 3c and the disinfection performance is shown in Fig. 3d. With infrared light alone, the disinfection efficiency (83%) was much less than that of visible light combined with infrared light together (>99.999%). Additionally, a temperature-control experiment also eliminated the thermal effect (Supplementary Fig. 5). Therefore, it is confirmed that visible-light photocatalysis

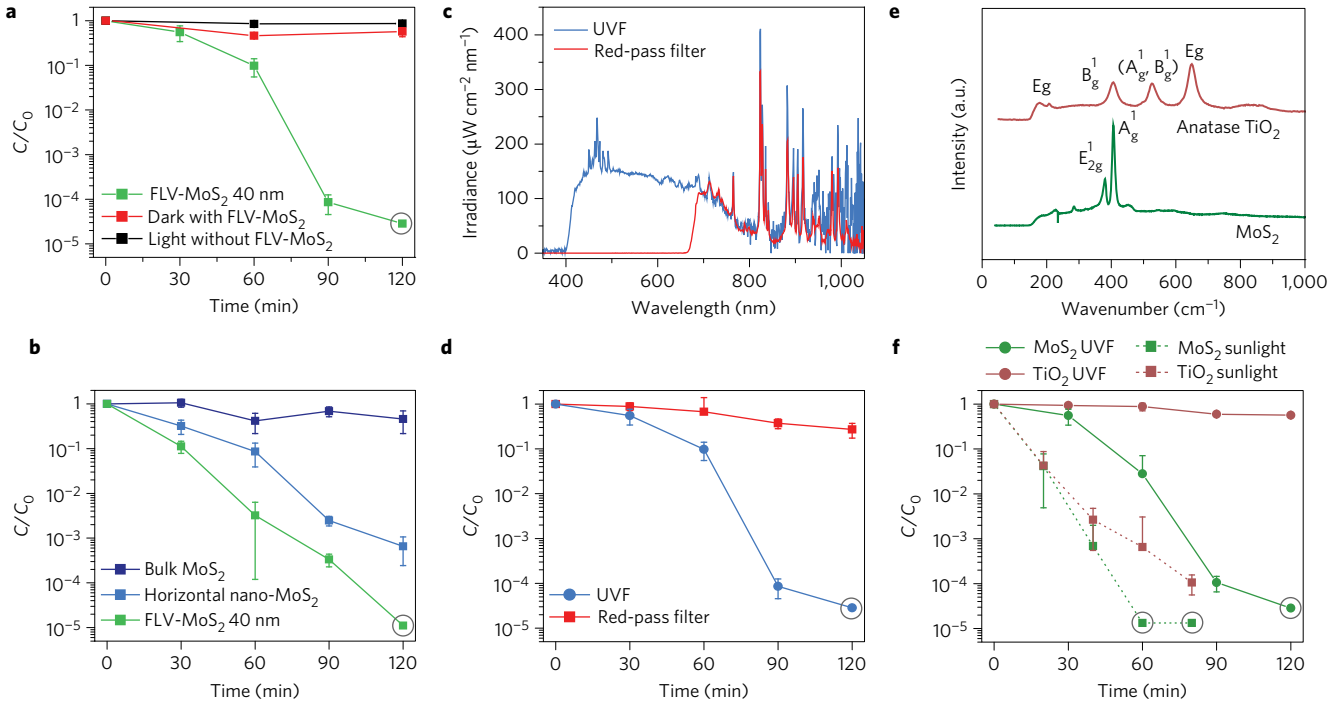


**Figure 3 | FLV-$MoS_2$ disinfection performance. a**, Comparison of the disinfection performances of FLV-$MoS_2$ with both light control without FLV-$MoS_2$ and FLV-$MoS_2$ in the dark to confirm the visible-light photocatalytic effect. **b**, Disinfection performances of FLV-$MoS_2$ compared with those of horizontal nano-$MoS_2$ and bulk $MoS_2$. **c**, Spectra of illuminating light sources, solar simulator with a UVF and solar simulator with a red-pass filter. **d**, Disinfection performances using different light sources, the solar simulator with a UVF and the solar simulator with a red-pass filter. **e**, Raman spectra of FLV-$MoS_2$ and $TiO_2$ films. **f**, Comparison of disinfection performance between FLV-$MoS_2$ and $TiO_2$ films under both visible-light and real-sunlight illumination. In the disinfection performances, the error bars represent the s.d. of three replicate measurements and the data point with a grey circle means no live bacteria were detected. a.u., arbitrary units.

instead of a thermal effect induces most of the disinfection. The disinfection effect of FLV-$MoS_2$ on a model Gram positive bacterium, *Enterococcus faecalis*, and another strain of *E. coli* was also demonstrated. No live bacteria were detected after 120 min of illumination (Supplementary Figs 6 and 7). This suggests that FLV-$MoS_2$ can be used to inactivate a variety of bacteria.

The disinfection performance of FLV-$MoS_2$ was compared with that of the well-studied photocatalyst $TiO_2$. $TiO_2$ film was grown through the atomic-layer-deposition method followed by an annealing process. The thickness of $TiO_2$ was kept the same as that of FLV-$MoS_2$. The Raman spectra of both FLV-$MoS_2$ and $TiO_2$ are shown in Fig. 3e and $TiO_2$ was confirmed to be in the anatase phase. A comparison of the disinfection performances of FLV-$MoS_2$ and $TiO_2$ is shown in Fig. 3f. Owing to the large 3.2 eV bandgap of $TiO_2$ (which corresponds to a light wavelength of 387 nm), illumination under the solar spectrum with an ultraviolet-light filter (UVF) did not induce any photocatalytic ROS generation. Hence, the *E. coli* concentration decreased just 44% after 120 min of illumination, which is similar to that of the light control. This confirms that $TiO_2$ was unable to harvest visible light for photocatalytic water disinfection. Using real sunlight as the light source (13:00 local time, 30 March 2013, Stanford, California—the spectrum is given in Supplementary Fig. 8), the disinfection performances of FLV-$MoS_2$ and $TiO_2$ were also compared (Fig. 3f). FLV-$MoS_2$ showed a 5 log inactivation of bacteria concentration (>99.999% inactivation efficiency) and no live bacteria were detected within 60 min of real-sunlight illumination. This gives a first-order disinfection rate of 0.18 $min^{-1}$ ($R^2 = 0.99$) for FLV-$MoS_2$ under real sunlight. $TiO_2$ showed a log inactivation efficiency of 3 log (99.9%) in 60 min, which corresponds to a disinfection rate of 0.12 $min^{-1}$ ($R^2 = 0.96$). Thus, the photocatalytic effect of FLV-$MoS_2$ was much better than that of $TiO_2$ for *E. coli* disinfection under both visible light and real sunlight.

## Disinfection performance enhanced by additional catalysts

Normally, the performance of a photocatalyst is governed by two critical properties, namely (1) the utilization of the solar spectrum by the semiconductor photocatalyst and (2) the efficacy of the generated electron–hole pairs for ROS production. For the second property, there is competition between the generated electrons and holes to produce ROS and other physical processes, such as electron–hole recombination, trapping in the material during diffusion and participating in other reactions (such as hydrogen evolution, oxygen reduction and oxidation). Semiconductor materials are usually non-specific in catalysing ROS production. Hence, to promote the production of ROS, the addition of catalysts is crucial. Nano-size noble metals are used to decorate the semiconductor material surface to serve as ROS catalysts and to form metal–semiconductor junctions to enhance electron–hole separation. It has been shown in the literature that, with the addition of nanosize noble metals, ROS production can be increased dramatically[45–47].

To accelerate the photocatalytic disinfection rate, 5 nm of Cu or Au was deposited onto the FLV-$MoS_2$ to catalyse the ROS generation and also to improve the electron–hole pair separation. Cu and Au are good catalysts for ROS generation and they preferentially catalyse the two-electron oxygen reduction reaction for $H_2O_2$ generation over a four-electron transfer reaction (Supplementary Fig. 9). Cu and Au are deposited via a thermal evaporation process. The morphologies of as-grown Cu–$MoS_2$ and Au–$MoS_2$ were characterized by TEM and scanning electron microscopy (SEM), and the images are shown in Fig. 4a and Supplementary Fig. 10. The thermal evaporation process did not change the morphology of the $MoS_2$ film. No obvious intercalations of Cu or Au were observed because the layer spacing was ~0.63 nm and ~0.62 nm for Cu–$MoS_2$ and Au–$MoS_2$, respectively, which is similar to that of pristine FLV-$MoS_2$, ~0.60 nm (Supplementary Fig. 11). The existence of the Cu and Au films was

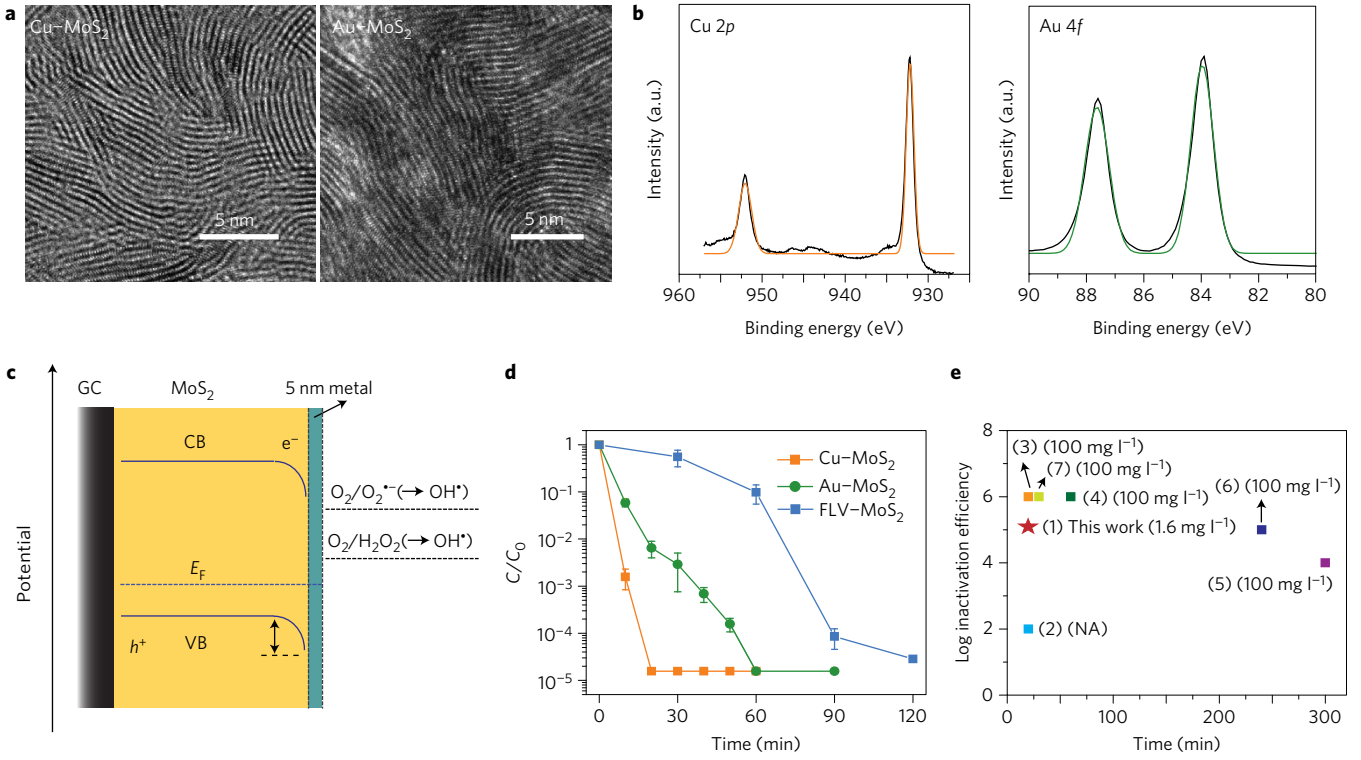


**Figure 4 | Performance enhancement of FLV-$MoS_2$ by 5 nm of catalysts of Cu or Au. a**, TEM images (top view) show the morphology of Cu-$MoS_2$ and Au-$MoS_2$ after deposition. **b**, XPS characterization of Cu-$MoS_2$ and Au-$MoS_2$ shows the presence of Cu and Au. **c**, Schematic that shows the enhancement of electron–hole separation to facilitate the electrons to participate in ROS-generation reactions after Cu/Au deposition. **d**, Disinfection-performance comparison of Cu-$MoS_2$ and Au-$MoS_2$ with pristine FLV-$MoS_2$ shows the rapid disinfection by Cu-$MoS_2$ and Au-$MoS_2$ after deposition of the catalysts. **e**, Disinfection-performance comparison of Cu-$MoS_2$ with the literature values of other photocatalysts using *E. coli*. The plot shows the log inactivation of *E. coli* with respect to illumination time for all the photocatalysts in the comparison: (1) Cu-$MoS_2$ (this work, 2 $cm^2$ film equivalent to 1.6 mg $l^{-1}$), (2) $TiO_2$–CdS (ref. 25) (1 $cm^2$ film), (3) ZnO/Cu (ref. 48) (100 mg $l^{-1}$), (4) GO-CdS (ref. 34) (100 mg $l^{-1}$), (5) BV (ref. 36) (100 mg $l^{-1}$), (6) GO-$C_3N_4$ (ref. 37) (100 mg $l^{-1}$) and (7) SGO-ZnO-Ag (ref. 35) (100 mg $l^{-1}$). Details of the conditions for the photocatalytic-disinfection experiments (sample concentration, light source and intensity, and bacteria strain) are given in Supplementary Table 1. The final inactivation efficiencies are limited by the initial bacterial concentration. NA, not available.

confirmed by X-ray photoelectron spectroscopy (XPS) (Fig. 4b). The XPS data showed signature peaks for Cu $2p_{3/2}$ at 932.6 eV and for Au $4f_{7/2}$ at 83.9 eV. Besides the catalytic effect, Cu and Au can also increase the separation of electron–hole pairs. The work functions of Cu and Au are 4.7 and 5.1 eV, respectively. When in contact with p-type FLV-$MoS_2$, the Schottky junction facilitates the electron migration to the Cu or Au surface and the electrons participate in the oxygen-reduction reactions to produce ROS, as explained in the schematic in Fig. 4c. This should further promote the oxygen-reduction reaction for ROS generation.

The disinfection performances of Cu–$MoS_2$ and Au–$MoS_2$ are shown in Fig. 4d. A solar simulator with a UVF was used as the light source, as in the disinfection experiments. For FLV-$MoS_2$ without any catalyst, after 120 min of illumination no live *E. coli* were detected. With 5 nm of Cu, the disinfection rate was enhanced and within only 20 min no live bacteria were detected, which is equivalent to a disinfection efficiency of >99.999%. For Au–$MoS_2$, the illumination time to achieve >99.999% disinfection efficiency was also shortened relative to FLV-$MoS_2$ to 60 min. The disinfection rates for Cu–$MoS_2$ and Au–$MoS_2$ were 0.57 $min^{-1}$ ($R^2 = 0.99$) and 0.19 $min^{-1}$ ($R^2 = 0.96$), respectively, under a solar simulator with a UVF. These are much faster compared with that of FLV-$MoS_2$, 0.087 $min^{-1}$ ($R^2 = 0.99$). The disinfection enhancement confirmed the efficacy of Cu and Au to separate electron–hole pairs more efficiently and catalyse the oxygen reduction reactions for ROS generation. With Cu and Au as catalysts the disinfection rate is enhanced sixfold and twofold, respectively. After the photocatalytic disinfection experiments, the concentration of Cu or Au was measured. No detectable Au was present in the water sample and the Cu concentration was 3.25 ppb (μg $l^{-1}$), which is <1% of the Cu catalyst mass loading.

## Photocatalytic disinfection mechanism

Furthermore, to prove directly the disinfection mechanism by ROS in the FLV-$MoS_2$ and Cu–$MoS_2$ systems, and also to prove the catalytic effect of Cu, ROS concentrations in both systems were measured and a series of ROS-scavenging experiments were conducted. The results are shown in Supplementary Figs 12–14 and Supplementary Discussion. It was shown that four ROS ($O_2^{\bullet-}$, $^1O_2$, $H_2O_2$ and $OH^{\bullet}$) were present in both the FLV-$MoS_2$ and Cu–$MoS_2$ systems with concentrations of $H_2O_2 > O_2^{\bullet-} > {}^1O_2 > OH^{\bullet}$. Moreover, for each ROS, the concentration in the Cu–$MoS_2$ system was higher than that in the FLV-$MoS_2$ system. This is consistent with the fact that Cu–$MoS_2$ demonstrated a higher disinfection rate and also proves the effectiveness of Cu in catalysing ROS generation. Six scavenger-quenching experiments were conducted to study the disinfection contribution of each ROS as well as of the electrons and holes. The results suggest that $H_2O_2$ has the strongest effect in inactivating bacteria, and that oxygen-reduction-related ROS dominates the disinfection effect. All these results are consistent with the band structure of $MoS_2$, which favours oxygen reduction to produce ROS. Also, FLV-$MoS_2$ and Cu–$MoS_2$ proved to be stable after multicycle tests (Supplementary Fig. 15).

The bacterial disinfection performance of Cu–$MoS_2$, with a disinfection rate of 0.57 $min^{-1}$ ($R^2 = 0.99$) under a solar simulator with a UVF is, so far, among the best based on a review of the literature in terms of speed and log reduction in bacterial concentration (Fig. 4e and Supplementary Table 1). Compared with those that achieve total disinfection (no live bacteria detected) within 30 min, such as ZnO/Cu (ref. 48), graphene oxide (GO)–CdS (ref. 34) and sulfonated graphene oxide (SGO)–ZnO–Ag (ref. 35), the material mass loading used in the case of Cu–$MoS_2$ is ~60 times less than that of the others. However, for fixed photocatalysts grown on substrates with a similar material mass loading, such as $TiO_2$–CdS (ref. 25), the disinfection rate of Cu–$MoS_2$ (>99.999%) is much faster than that of $TiO_2$–CdS (~90%) in 20 min. Hence Cu–$MoS_2$ shows great advantage as a new effective visible-light photocatalyst for water disinfection.

In conclusion, we have demonstrated the efficient harvesting of visible light for photocatalytic water disinfection with a novel material, FLV-$MoS_2$. By decreasing the domain size, the bandgap of $MoS_2$ was increased from 1.3 eV (bulk material) to 1.55 eV (FLV-$MoS_2$). This enabled the FLV-$MoS_2$ to generate ROS successfully for bacteria inactivation in water. The FLV-$MoS_2$ showed a faster disinfection than the most-studied photocatalyst, $TiO_2$. With the additional deposition of Cu or Au to assist electron–hole pair separation and also to catalyse the ROS production reactions, FLV-$MoS_2$ showed a rapid inactivation of >99.999% bacteria in only 20 or 60 min, respectively. The promising performance of FLV-$MoS_2$ and Cu–$MoS_2$ on bacteria shows great potential as photocatalysts for the visible-light inactivation of pathogens (bacteria, viruses and protozoa) in water.

## Methods

Methods and any associated references are available in the online version of the paper.

Received 16 December 2015; accepted 28 June 2016; published online 15 August 2016

## References


1. Shannon, M. A. *et al.* Science and technology for water purification in the coming decades. *Nature* **452,** 301–310 (2008).
2. Schwarzenbach, R. P. *et al.* The challenge of micropollutants in aquatic systems. *Science* **313,** 1072–1077 (2006).
3. Liu, C. *et al.* Conducting nanosponge electroporation for affordable and high-efficiency disinfection of bacteria and viruses in water. *Nano Lett.* **13,** 4288–4293 (2013).
4. Liu, C. *et al.* Static electricity powered copper oxide nanowire microbicidal electroporation for water disinfection. *Nano Lett.* **14,** 5603–5608 (2014).
5. Logan, B. E. & Elimelech, M. Membrane-based processes for sustainable power generation using water. *Nature* **488,** 313–319 (2012).
6. McGuigan, K. G. *et al.* Solar water disinfection (SODIS): a review from bench-top to roof-top. *J. Hazard. Mater.* **235,** 29–46 (2012).
7. Sinha, R. P. & Hader, D. P. UV-induced DNA damage and repair: a review. *Photochem. Photobiol. Sci.* **1,** 225–236 (2002).
8. Hijnen, W. A. M., Beerendonk, E. F. & Medema, G. J. Inactivation credit of UV radiation for viruses, bacteria and protozoan (oo)cysts in water: a review. *Water Res.* **40,** 3–22 (2006).
9. Silverman, A. I., Peterson, B. M., Boehm, A. B., McNeill, K. & Nelson, K. L. Sunlight inactivation of human viruses and bacteriophages in coastal waters containing natural photosensitizers. *Environ. Sci. Technol.* **47,** 1870–1878 (2013).
10. Dong, S. Y. *et al.* Recent developments in heterogeneous photocatalytic water treatment using visible light-responsive photocatalysts: a review. *RSC Adv.* **5,** 14610–14630 (2015).
11. Dong, S. Y. *et al.* Designing three-dimensional acicular sheaf shaped $BiVO_4$/reduced graphene oxide composites for efficient sunlight-driven photocatalytic degradation of dye wastewater. *Chem. Eng. J.* **249,** 102–110 (2014).
12. Dong, S. Y. *et al.* $ZnSnO_3$ hollow nanospheres/reduced graphene oxide nanocomposites as high-performance photocatalysts for degradation of metronidazole. *Appl. Catal. B* **144,** 386–393 (2014).
13. Chong, M. N., Jin, B., Chow, C. W. K. & Saint, C. Recent developments in photocatalytic water treatment technology: a review. *Water Res.* **44,** 2997–3027 (2010).
14. Malato, S., Fernandez-Ibanez, P., Maldonado, M. I., Blanco, J. & Gernjak, W. Decontamination and disinfection of water by solar photocatalysis: recent overview and trends. *Catal. Today* **147,** 1–59 (2009).
15. Wardman, P. Reduction potentials of one-electron couples involving free-radicals in aqueous-solution. *J. Phys. Chem. Ref. Data* **18,** 1637–1755 (1989).
16. Wood, P. M. The potential diagram for oxygen at pH-7. *Biochem. J.* **253,** 287–289 (1988).
17. Lawless, D., Serpone, N. & Meisel, D. Role of $OH^{\bullet}$ radicals and trapped holes in photocatalysis—a pulse radiolysis study. *J. Phys. Chem.* **95,** 5166–5170 (1991).
18. Liao, H. D. & Reitberger, T. Generation of free $OH_{aq}$ radicals by black light illumination of Degussa (Evonik) P25 $TiO_2$ aqueous suspensions. *Catalysts* **3,** 418–443 (2013).
19. Chen, X. & Mao, S. S. Titanium dioxide nanomaterials: synthesis, properties, modifications, and applications. *Chem. Rev.* **107,** 2891–2959 (2007).
20. Li, Q., Xie, R. C., Ll, Y. W., Mintz, E. A. & Shang, J. K. Enhanced visible-light-induced photocatalytic disinfection of *E. coli* by carbon-sensitized nitrogen-doped titanium oxide. *Environ. Sci. Technol.* **41,** 5050–5056 (2007).
21. Cong, Y., Zhang, J. L., Chen, F., Anpo, M. & He, D. N. Preparation, photocatalytic activity, and mechanism of nano-$TiO_2$ co-doped with nitrogen and iron (III). *J. Phys. Chem. C* **111,** 10618–10623 (2007).
22. Asahi, R., Morikawa, T., Ohwaki, T., Aoki, K. & Taga, Y. Visible-light photocatalysis in nitrogen-doped titanium oxides. *Science* **293,** 269–271 (2001).
23. Choi, J., Park, H. & Hoffmann, M. R. Effects of single metal-ion doping on the visible-light photoreactivity of $TiO_2$. *J. Phys. Chem. C* **114,** 783–792 (2010).
24. Yu, J. C. *et al.* Efficient visible-light-induced photocatalytic disinfection on sulfur-doped nanocrystalline titania. *Environ. Sci. Technol.* **39,** 1175–1179 (2005).
25. Hayden, S. C., Allam, N. K. & El-Sayed, M. A. $TiO_2$ nanotube/CdS hybrid electrodes: extraordinary enhancement in the inactivation of *Escherichia coli*. *J. Am. Chem. Soc.* **132,** 14406–14408 (2010).
26. Chen, C. *et al.* Synthesis of visible-light responsive graphene oxide/$TiO_2$ composites with p/n heterojunction. *ACS Nano* **4,** 6425–6432 (2010).
27. Yu, J. G., Dai, G. P. & Huang, B. B. Fabrication and characterization of visible-light-driven plasmonic photocatalyst Ag/AgCl/$TiO_2$ nanotube arrays. *J. Phys. Chem. C* **113,** 16394–16401 (2009).
28. Mor, G. K., Varghese, O. K., Paulose, M., Shankar, K. & Grimes, C. A. A review on highly ordered, vertically oriented $TiO_2$ nanotube arrays: fabrication, material properties, and solar energy applications. *Sol. Energy Mater. Sol. Cells* **90,** 2011–2075 (2006).
29. Tao, J. G., Luttrell, T. & Batzill, M. A two-dimensional phase of $TiO_2$ with a reduced bandgap. *Nature Chem.* **3,** 296–300 (2011).
30. Dette, C. *et al.* $TiO_2$ anatase with a bandgap in the visible region. *Nano Lett.* **14,** 6533–6538 (2014).
31. Huang, J. H., Ho, W. K. & Wang, X. C. Metal-free disinfection effects induced by graphitic carbon nitride polymers under visible light illumination. *Chem. Commun.* **50,** 4338–4340 (2014).
32. Wang, X. C. *et al.* A metal-free polymeric photocatalyst for hydrogen production from water under visible light. *Nature Mater.* **8,** 76–80 (2009).
33. Xia, D. H. *et al.* Red phosphorus: an Earth-abundant elemental photocatalyst for 'green' bacterial inactivation under visible light. *Environ. Sci. Technol.* **49,** 6264–6273 (2015).
34. Gao, P., Liu, J. C., Sun, D. D. & Ng, W. Graphene oxide–CdS composite with high photocatalytic degradation and disinfection activities under visible light irradiation. *J. Hazard. Mater.* **250,** 412–420 (2013).
35. Gao, P., Ng, K. & Sun, D. D. Sulfonated graphene oxide–ZnO–Ag photocatalyst for fast photodegradation and disinfection under visible light. *J. Hazard. Mater.* **262,** 826–835 (2013).
36. Wang, W. J. *et al.* Visible-light-driven photocatalytic inactivation of *E. coli* K-12 by bismuth vanadate nanotubes: bactericidal performance and mechanism. *Environ. Sci. Technol.* **46,** 4599–4606 (2012).
37. Wang, W. J., Yu, J. C., Xia, D. H., Wong, P. K. & Li, Y. C. Graphene and g-$C_3N_4$ nanosheets co-wrapped elemental α-sulfur as a novel metal-free heterojunction photocatalyst for bacterial inactivation under visible-light. *Environ. Sci. Technol.* **47,** 8724–8732 (2013).
38. Radisavljevic, B., Radenovic, A., Brivio, J., Giacometti, V. & Kis, A. Single-layer $MoS_2$ transistors. *Nature Nanotechnol.* **6,** 147–150 (2011).
39. Wang, Q. H., Kalantar-Zadeh, K., Kis, A., Coleman, J. N. & Strano, M. S. Electronics and optoelectronics of two-dimensional transition metal dichalcogenides. *Nature Nanotechnol.* **7,** 699–712 (2012).
40. Jaramillo, T. F. *et al.* Identification of active edge sites for electrochemical $H_2$ evolution from $MoS_2$ nanocatalysts. *Science* **317,** 100–102 (2007).
41. Kong, D. S. *et al.* Synthesis of $MoS_2$ and $MoSe_2$ films with vertically aligned layers. *Nano Lett.* **13,** 1341–1347 (2013).
42. Wang, H. T. *et al.* Electrochemical tuning of vertically aligned $MoS_2$ nanofilms and its application in improving hydrogen evolution reaction. *Proc. Natl Acad. Sci. USA* **110,** 19701–19706 (2013).
43. Mak, K. F., Lee, C., Hone, J., Shan, J. & Heinz, T. F. Atomically thin $MoS_2$: a new direct-gap semiconductor. *Phys. Rev. Lett.* **105,** 136805 (2010).
44. Tong, H. *et al.* Nano-photocatalytic materials: possibilities and challenges. *Adv. Mater.* **24,** 229–251 (2012).

45. Sakthivel, S. *et al.* Enhancement of photocatalytic activity by metal deposition: characterisation and photonic efficiency of Pt, Au and Pd deposited on $TiO_2$ catalyst. *Water Res.* **38,** 3001–3008 (2004).
46. Li, H. X. *et al.* Mesoporous Au/$TiO_2$ nanocomposites with enhanced photocatalytic activity. *J. Am. Chem. Soc.* **129,** 4538–4539 (2007).
47. Subramanian, V., Wolf, E. E. & Kamat, P. V. Catalysis with $TiO_2$/gold nanocomposites. Effect of metal particle size on the Fermi level equilibration. *J. Am. Chem. Soc.* **126,** 4943–4950 (2004).
48. Bai, H. W., Liu, Z. Y. & Sun, D. D. Hierarchical ZnO/Cu 'corn-like' materials with high photodegradation and antibacterial capability under visible light. *Phys. Chem. Chem. Phys.* **13,** 6205–6210 (2011).

## Acknowledgements

We acknowledge the Stanford facilities, Stanford Nanocharacterization Laboratory and Soft & Hybrid Materials, for characterization. Y.C. acknowledges support from the US Department of Energy, Basic Energy Sciences, Materials Sciences and Engineering Division, under contract DE-AC02-76SF00515. We thank G. M. Stewart for his help with the schematic drawing.

## Author contributions

C.L. and Y.C. developed the concept. C.L. synthesized the samples and conducted the disinfection measurement and material characterizations. D.K. and H.W. helped with the material synthesis. P.-C.H. and S.W. helped with the optical measurement. H.Y. helped with the Kelvin probe measurement. H.-W.L. did the TEM characterization. D.K. helped with the Raman spectroscopy measurement. Y.L. helped with catalyst measurements. P.A.M. helped with estimation of the real-sunlight spectrum. K.M.P. helped with HPLC measurement. C.L., A.B.B. and Y.C. analysed the data and co-wrote the paper. K.Y. and D.L. provided important experimental insights. All the authors discussed the whole paper.

## Additional information

Supplementary information is available in the online version of the paper. Reprints and permissions information is available online at www.nature.com/reprints. Correspondence and requests for materials should be addressed to Y.C.

## Competing financial interests

The authors declare no competing financial interests.

## Methods

**FLV-$MoS_2$ growth.** Edge-terminated $MoS_2$ films were grown inside a single-zone, 12 inch horizontal tube furnace (Lindberg/Blue M) equipped with a 1 inch diameter quartz tube. For the 40 nm FLV-$MoS_2$ film, the substrates (1 × 2 cm) were sputtered with a 10 nm thick Mo film as a precursor and then sulfurization at a base pressure of 100 mTorr Ar environment. The tube furnace was quickly raised to the reaction temperature of 500 °C in 20 min and kept at 500 °C for 10 min of reaction[41].

**Disinfection performance.** Bacteria (*E. coli* (JM109, Promega and ATCC K-12) and *Enterococcus faecalis* (ATCC 19433)), were cultured to log phase, harvested by centrifugation at 900*g*, washed twice with deionized (DI) water and suspended in DI water to ~$10^6$ c.f.u. $ml^{-1}$. Photocatalytic disinfection was performed using a solar simulator (Newport) calibrated at air mass 1.5G (100 mW $cm^{-2}$) as the light source and a UVF (Clarex) and red-pass filter (Clarex NIR-70) to tune the light spectrum. The FLV-$MoS_2$ sample size was 1 cm × 2 cm × 40 nm and the water volume was 25 ml. Bacterial concentrations were measured at different times of illumination using standard spread-plating techniques. Each sample was serially diluted and each dilution was plated in triplicate onto trypticase soy agar and incubated at 37 °C for 18 h. The experiments for the solar-disinfection performance were conducted in duplicate. The light spectra (solar simulator with a UVF or solar simulator with a red-pass filter) were measured at the same place at which the sample was set during the disinfection experiment. The solar spectrum during the real-sunlight experiment was estimated using a simple model of the atmospheric radiative transfer of sunshine. The disinfection rates ($k$) were estimated using Chick's law: $\ln(C/C_0) = -kt$ where $k$ is in units of per time, $C$ is the concentration of bacteria and $C_0$ is the concentration at $t = 0$ of the experiments. The slope of the line of best fit to $\ln(C/C_0)$ versus $t$ for each experiment was used to estimate $k$.

**Material characterization.** Characterizations were carried out using TEM (aberration-corrected FEI 80-300 environmental Titan (S) TEM microscope at 300 keV), Raman spectroscopy (WITEC Raman spectrometer), XPS (SSI SProbe XPS spectrometer with an Al Kα source), SEM (FEI Nova NanoSEM 450) and a scanning Kelvin probe (KP Technology Model 5050). The absorption measurement used a xenon lamp (69911, Newport) as the light source coupled with a monochromator (74125, Newport).